# High-Performance Photoresponsive Organic Nanotransistors with Single-Layer Graphenes as Two-Dimensional Electrodes

By *Yang Cao, Song Liu, Qian Shen, Kai Yan, Pingjian Li, Jun Xu, Dapeng Yu, Michael L. Steigerwald, Colin Nuckolls, Zhongfan Liu,** and *Xuefeng Guo**

**Graphene behaves as a robust semimetal with the high electrical conductivity stemming from its high-quality tight two-dimensional crystallographic lattice. It is therefore a promising electrode material. Here, a general methodology for making stable photoresponsive field effect transistors, whose device geometries are comparable to traditional macroscopic semiconducting devices at the nanometer scale, using cut graphene sheets as 2D contacts is detailed. These contacts are produced through oxidative cutting of individual 2D planar graphene by electron beam lithography and oxygen plasma etching. Nanoscale organic transistors based on graphene contacts show high-performance FET behavior with bulk-like carrier mobility, high on/off current ratio, and high reproducibility. Due to the presence of photoactive molecules, the devices display reversible changes in current when they are exposed to visible light. The calculated responsivity of the devices is found to be as high as ~8.3 A $W^{-1}$. This study forms the basis for making new types of ultrasensitive molecular devices, thus initiating broad research interest in the field of nanoscale/molecular electronics.**

## 1. Introduction

There has been tremendous effort directed at making nanoscale transport junctions that enable the measurement of the electrical characteristics of single or small collections of organic molecules,[1–11] the ultimate goal being single molecule/atom transistors.[2,12–14] To reach this goal, it is important to develop materials and paradigms for device architecture and operation to optimize intrinsic function in devices needed for high carrier mobility and high gate efficiency. New forms of carbon, such as single-walled carbon nanotubes (SWNTs)[15–16] and graphene,[17–18] have emerged as promising materials for use in these devices.

In recent work, we have demonstrated that SWNTs can function as efficient point contacts[19–23] for nanoscale field-effect transistors (FETs). We made organic FETs out of both monolayers and self-assembled columns[24] of polycyclic aromatic hydrocarbons. These devices are ultrasensitive to their chemical environment, temperature, and light.[25] Graphene, a newly isolated form of carbon, holds a set of remarkable electronic and physical properties that make them ideal for use in electronics[26–28] and its discovery has led to a deluge of worldwide research interest.[17–18,26–42] As an electrode for nanoscale electrical devices graphene is attractive because it is a very thin (single-atom thick), 2D semimetal that is easily available in very high crystallographic quality. We suggest that single-layer graphenes may prove to be another type of ideal electrodes for making a wide variety of molecular devices (Fig. 1) and might improve the performance of organic nano-FETs. In this article, we describe a new class of photoresponsive organic nano-transistors with device geometries comparable to traditional macroscopic semiconducting devices at the nanometer scale (Fig. 1). Particularly relevant to our design are the studies of Liu and co-workers,

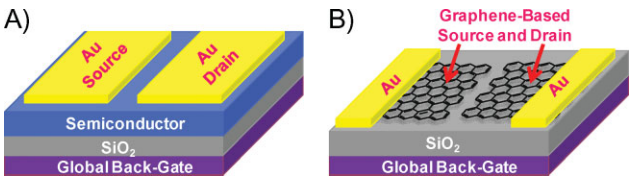


**Figure 1.** A schematic of comparable device geometries between A) traditional macroscopic FETs and B) FETs based on 2D graphene contacts.

[*] Prof. Z. Liu, Prof. X. Guo, Y. Cao, S. Liu, Q. Shen, K. Yan
Beijing National Laboratory for Molecular Sciences (BNLMS)
State Key Laboratory for Structural Chemistry of Unstable and Stable Species
College of Chemistry and Molecular Engineering, Peking University
Beijing 100871 (P. R. China)
E-mail: guoxf@pku.edu.cn; zfliu@pku.edu.cn
P. Li, J. Xu, Prof. D. Yu
College of Physics, Peking University
Beijing 100871 (P. R. China)
M. L. Steigerwald, Prof. C. Nuckolls
Department of Chemistry
The Columbia University Center for Electronics of Molecular Nanostructures
Columbia University
New York, NY 10027 (USA)

**DOI: 10.1002/adfm.200900408**

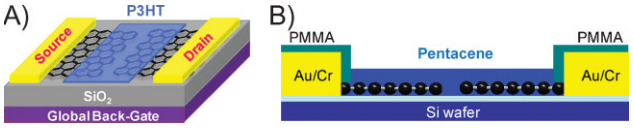


**Figure 2.** A schematic of how graphene sheets function as 2D electrodes to measure the electrical conductance of organic semiconductors. A) Device structure of P3HT transistors made by dip-coating. Only the nanogaps between graphene sheets are covered by P3HT. B) Device structure of pentacene transistors with graphene-metal junctions protected by PMMA.

which show that metal electrodes modified by CVD-grown multilayer graphenes show good electrode/organic interface contact and low hole-injection barrier, thus leading to improved organic FETs with macroscopic channel length.[43] Our devices directly use cut pristine 2D metallic, single-layer graphene sheets as nanoscale source/drain electrodes through ultra-fine electron beam lithography and precise oxygen plasma etching. After deposition of ordered, organic thin films [either poly (3-hexylthiopene-2,5-diyl) (P3HT) or pentacene] as the semiconductors (Fig. 2), these nano-transistors based on graphene contacts show high-performance FET behaviors with bulk-like carrier mobility, high on/off current ratio, and high reproducibility. Due to the presence of photosensitive organic materials, reversible significant changes in current were observed when the devices were exposed to visible light.

## 2. Results and Discussion

The fabrication of three-terminal graphene-based transistors is described in the Experimental Section.[26–28] In brief, graphene sheets are obtained by a repeated peeling-off technique on a heavily doped silicon substrate with a 300 nm layer of thermally grown oxide. Identification of the single graphene sheets is performed by a combination of optical and atomic force microscopy. Metallic electrodes (3 nm of Cr followed by 40 nm of Au) are formed on top of the graphene using thermal evaporation followed by electron beam lithography. The doped silicon wafer serves as a global back-gate electrode for the devices. We determine the electrical characteristics of these simple devices, and then we oxidatively cut individual graphene sheets using another ultrafine lithographic process and oxygen plasma etching. This produces nanogaps between the graphene half-sheets.[24,25] We controlled the fabrication procedure to give a gap size in the range of 100–150 nm. Given the dielectric thickness of 300 nm, this gap gives the shortest channel length that can yield an efficient field effect from the global back-gate.[44,45] We then deposit thin films of organic semiconductors within and across the gap between the graphene half-sheets. We test the electrical behavior of these devices by applying source/drain voltages ($V_D$) to the metal pads that are connected to the graphene sheets and measuring drain current $I_D$.[22–25] By applying gate bias voltage ($V_G$), we can fine-tune the carrier density in the devices.

In Figure 3A we show optical micrographs of a representative device and atomic force microscopic image of the graphene sheet within that device. The average thickness of graphenes used in this study is 0.5–0.9 nm, a single layer of graphene.[46,47] In the device shown in Figure 3 the width of the gap between the graphene half-sheets is ~100 nm. To aid in the subsequent analysis of the devices, we record the electrical characteristics of all the devices before and after the graphene is fully cut; Figure 3B shows the comparison of the electrical properties of the same device before and after the graphene is cut. Before cutting, the resistance of the device is ~1.12 KΩ (black) at $V_D = -500\,\mu V$ and $V_G = -20\,V$, and after cutting the circuit is now open with the current through the device at the noise limit of the measurement (~100 fA) (red). To obtain the best results, we must treat the devices at 380 °C under a constant flow of argon gas for an hour after the lithographic process. We assume this post-process annealing removes any residue of polymethylmethacrylate (PMMA) and otherwise cleans the graphene surfaces. Once the nanogaps are formed and cleaned, organic semiconductors are then deposited through dip-coating or thermal evaporation to form FETs.

To test the efficiency of graphene-based electrodes, the first molecule used in this work is one of the most commonly-used organic semiconductors, regioregular P3HT. To form the devices, we immerse the open graphene circuits (Fig. 2) in a dilute chloroform solution of P3HT (~0.25 mg mL$^{-1}$). The devices are removed from solution and dried under a stream of inert gas. All of the as-formed devices by dip-coating behaved as p-type

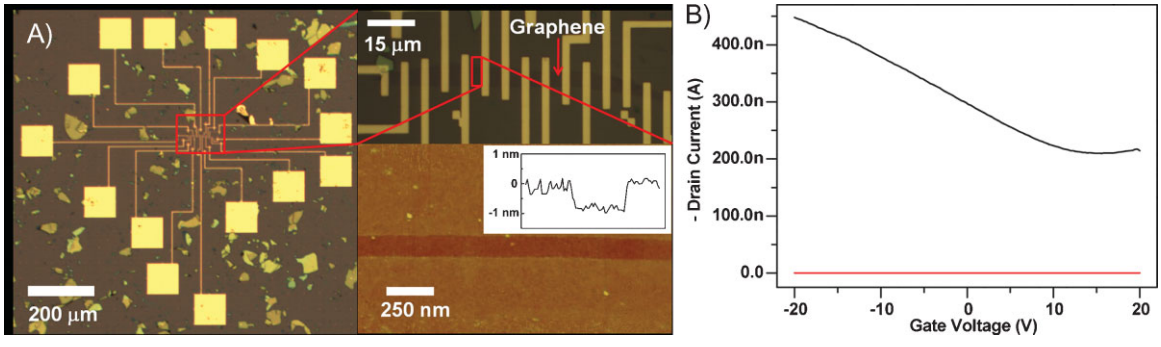


**Figure 3.** A) Optical micrographs and atomic force microscopic image of a representative device. The average thickness of graphenes used here is ~0.8 nm, a single layer of graphene. The gap size between the graphene ends is ~100 nm. Inset is the height profile across the nanogap. B) Electrical characteristics of the same graphene sheet ($I_D$ vs. $V_G$ at $V_D = -500\,\mu V$) used for testing before (black curve) and after (red curve) oxidative cutting. More details of another device can be found in the Supporting Information (Fig. S1).

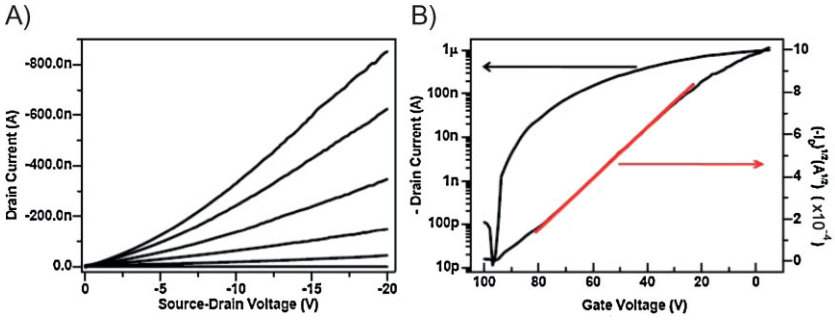


**Figure 4.** Device characteristics of a representative P3HT thin film transistor based on 2D graphene contacts in Figure 3A made by dip-coating from its dilute chloroform solution (~0.25 mg mL$^{-1}$). A) Transistor output, $V_G = 100$ to $-5$ V in $-21$ V steps. B) Transfer characteristics for the device, $V_D = -20$ V. The field effect mobility $\mu$, calculated in the red regime, is $\sim 1.4 \times 10^{-3}$ cm$^2$ V·s$^{-1}$ at $V_D = -20$ V. $L = \sim 100$ nm and $W = \sim 4$ μm.

semiconductors. Figure 4 shows the transistor characteristics for a representative device characterized in Figure 3. The results are reproducible as the yield of the working devices is quite good, ~68% out of ~50 devices. The field effect mobility ($\mu$) calculated using the standard method is among 0.9–1.5 $\times 10^{-3}$ cm$^2$ V·s$^{-1}$ with on/off current ratios of around five orders. These devices made from graphene-based electrodes are stable and their properties do not degrade after many measurement cycles.

In these devices, there are two possible pathways for charge transport.[25] The first is the traditional way, bypassing the graphene entirely, through the junctions between Au electrodes and P3HT thin films (as if in a device such as in Fig. 1A); the other is through the junctions between cut graphenes and P3HT molecules (Fig. 2A). In order to test the first possibility, systematic control experiments were performed. Control devices composed of only metal electrodes without graphene sheets and with the same device geometry as those in Figure 3A are fabricated by electron beam lithography (see the Supporting Information, Fig. S2A). P3HT thin films formed from solution with different concentrations (0.50, 0.30, 0.28, and 0.25 mg mL$^{-1}$) were dip-coated at room temperature on these control devices. We found that the yields of the working control devices gradually decreased from ~30% down to ~10%, ~5%, and at last zero out of ~20 devices separately for each concentration. None of the control devices formed from 0.25 mg mL$^{-1}$ solution show obvious FET properties. Typical device characteristics in devices formed from the solution with different concentrations can be found in the Supporting Information (Fig. S2). The dramatic decrease in the yields of the working control devices should be mainly ascribed to the low P3HT concentrations we used here that cannot efficiently bridge metal electrodes with the same device geometry. Since we use the 0.25 mg mL$^{-1}$ solution when we prepare our graphene-based devices, and since the graphene-based device yield is high (~68%), we suggest that the current path of the devices is through graphene electrodes bridged by P3HT.

It is remarkable to note that these molecular transistors, which utilize the 2D planar nanoscale graphene electrodes, display high current modulation and high on/off ratio. The on/off current ratio is as high as that of macroscopic organic FETs (~$10^5$ in Fig. 4). This ratio is one of the critical parameters evaluating the quality of organic FETs and has proven difficult to achieve in nanoscale devices made from metal electrodes.[48,49] Compared with metal electrodes, graphenes possess the molecular structure similar to organic semiconductors. Strong interaction between graphene and organic semiconductors might induce the self-assembly of the molecules in the conducting channel by $\pi$–$\pi$ interactions and lead to excellent interface contact. Graphite has a work function of ~4.4 eV,[50] which is 0.9 eV lower than that of Au.[51] Consequently, there is a low hole-injection barrier between graphene and organic layers. Both the excellent interface contact and the reduced injection barrier could result in the high-performance behaviors of the nanodevices. Such high on/off ratio was ever achieved in aromatic monolayer transistors using SWNT electrodes because of the 1D molecular structural nature of SWNTs.[24,25] In addition to the 2D planar structural nature of graphene electrodes, we think that the high electrical conductivity of semimetallic graphenes stemming from their perfect crystallographic structure plays an important role in device characteristics. Such devices with graphene-based contacts can function as bulk organic FETs and enable high-performance FET behaviors. Furthermore, because of the tight interatomic $sp^2$ bonds existing in their intrinsic structure without any defects, graphene-based electrodes are quite stiff, thus making devices robust even under the measurement of a source-drain voltage bias as high as $-20$ V. The calculated carrier mobility ($\mu$) is quite good albeit without further optimization, around $1.4 \times 10^{-3}$ cm$^2$ V·s$^{-1}$ at $V_D = -20$ V (within the red region in Fig. 4B, calculated using the standard method). Both of these values are comparable to those obtained from bulk organic FETs based on metal electrodes,[52–55] strongly suggesting that cut 2D planar graphene sheets can function as efficient electrodes, realizing the functions of macroscopic metal electrodes at the nanometer scale. We found that the threshold voltage ($V_T$) in these devices is approximately +95 V, a significant positive shift. This shift can be explained by the following equation:[56]

$$\Delta V_{th} \propto \exp\left[-\left(\frac{1}{\pi}\right)\left(\frac{\varepsilon_{ox}}{\varepsilon_{si}}\right)\left(\frac{L}{T_{ox}}\right)\right]$$

where $\varepsilon_{ox}$ is the dielectric constant of gate oxide, $\varepsilon_{si}$ the permittivity of Si, $L$ the channel length, and $T_{ox}$ is the gate oxide thickness. Thus the logarithm of the change in the threshold voltage ($V_T$) is proportional to the channel length ($L$) to a first approximation. When the channel length decreases to the thickness of gate oxide, the threshold voltage ($V_T$) changes dramatically. As a result, it is reasonable that $V_T$ in our devices shifts to the large positive value: our devices have channel lengths of 100–150 nm and oxide thicknesses of 300 nm. Another possibility is that the threshold voltage shift could also result from the high density of carrier traps at the interface between bare $SiO_2$ and P3HT. The experiments detailed here do not allow us to distinguish between the two explanations.

In the device depicted in Figure 2A, it is possible that the organic semiconductor makes contact directly to Au/Cr electrodes,

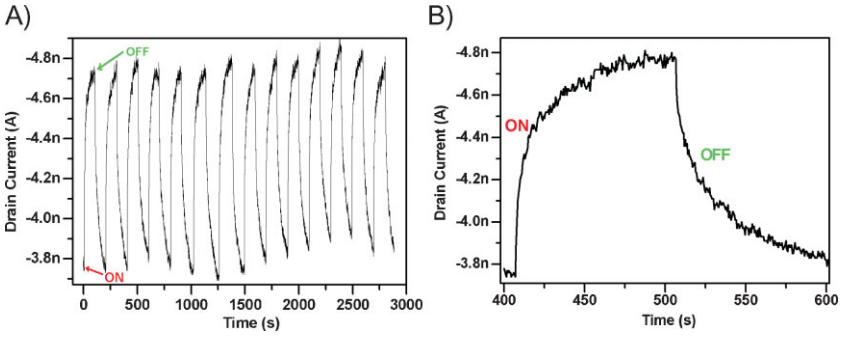


**Figure 5.** A) A time trace of the drain current for the same device used in Figure 4, showing the reversible photocurrent while the device was held at −2 V source-drain bias and −2 V gate bias by switching on/off light. B) A representative full switching cycle showing the quick saturation process in drain current of the device under light irradiation.

therefore it is possible that the device current bypasses the graphene entirely. To thoroughly ensure that the current path is through the cut graphene sheets and not through the macroscopic gold electrodes, we made transistors whose junctions between metal electrodes and graphene are protected by PMMA (Fig. 2B). After the graphene was fully cut, we coated the devices with PMMA and then using electron-beam lithography we opened a small window in the PMMA to expose just the graphene-based contacts. The optical micrographs of a representative pattern can be found in the Supporting Information (Fig. S3A). We then thermally evaporated pentacene (40 nm) on the top of the device stack. The details of the transistor characteristics for a device are listed in the Supporting Information (Fig. S3). These pentacene/graphene thin film transistors showed similar p-type FET properties, clearly proving that graphene–molecule–graphene junctions (GMGJs) are responsible for the electrical characteristics in devices. In this case, however, these pentacene devices displayed the relatively poor FET behavior because it was impossible to remove the residue of PMMA through annealing after the lithographic process, thus leading to a large contact resistance between pentacene and graphene sheets.

It is very interesting that these graphene-based transistors are sensitive to visible light because of the presence of photoactive organic materials.[57–59] We measured DC photoconductivity at room temperature in ambient atmosphere by illuminating the devices with visible light from a 150 W halogen lamp. Figure 5A shows the electrical photoresponse of the same device in Figure 4 made by dip-coating from the dilute chloroform solution of P3HT (~0.25 mg mL$^{-1}$). We can monitor the drain current as a function of time (with $V_D = V_G = -2$ V) by switching the light on and off. The reversible photocurrent, presumably originating from the photoexcited states of the molecules, was stable without any degradation for many measurement cycles even in the presence of oxygen and moisture in the air. Within a very short time, the drain current of the device saturated, indicating that the photoinduced carrier density reaches its maximum as shown in Figure 5B. The calculated responsivity of the device is very high, ~8.3 A W$^{-1}$ ($L$ = ~100 nm and $W$ = ~4 μm, $V_D = -2$ V and $V_G = -2$ V) at an intensity of 30 mW cm$^{-2}$, using the conventional model for the calculation.[60] To identify the reliability and generality of the device photoresponsiveness, we used the junction-protected devices as shown in Figure 2B to do the similar experiments. Figure S3E of the Supporting Information shows the drain current as a function of time of the same junction-protected device in Figure S3 ($V_G = V_D = -0.5$ V) by switching the light on and off. We also observed the quick, stable photoinduced current increase in the device upon exposure to visible light in the same condition, although its responsivity is relatively low, approximately $4.9 \times 10^{-2}$ A W$^{-1}$ ($L$ = ~120 nm and $W$ = ~4 μm, $V_D = -0.5$ V and $V_G = -0.5$ V) at an intensity of 30 mW cm$^{-2}$. The photoresponsive performance of these devices could be largely improved after further device optimization since graphene sheets can form the excellent interface contacts with organic semiconductors. To rule out potential artifacts, we carried out the similar experiments by using devices that have been fully cut, but lack active organic molecules. All of these devices behave as open circuits with no field effect induced by the gate electrode. A time trace for such a representative device is shown in the Supporting Information (Fig. S4). We also tested the bare graphene FET devices under similar conditions. There are no significant changes in the conductivity while visible light is switched. These results clearly prove that active organic materials (P3HT and pentacene) play the key role in device characteristics, thus opening a path to ultrasensitive devices based on novel 2D graphene electrodes for environmental sensing and solar energy harvesting.

## 3. Conclusions

In conclusion, we have outlined a straightforward methodology for making high-performance photosensitive nanoscale transistors based on 2D single-layer graphene contacts. These contacts are directly prepared by the oxidative cutting of an individual 2-dimensional planar graphene sheet by electron beam lithography and oxygen plasma etching. Because of the 2D nature of graphene, efficacious transistors at the nanometer scale, whose device geometries are comparable to traditional organic FETs, are readily formed through standard techniques. We used a common organic semiconductor (P3HT) to form transistors by dip-coating from solution. Due to the molecular structure and the high electrical conductivity of robust semimetallic graphenes, these devices showed high-performance FET behaviors with high on/off ratios and bulk-like carrier mobilities. We also developed another type of device geometry, forming pentacene thin film transistors where junctions between metal electrodes and graphenes have been protected by PMMA. These so-formed pentacene transistors showed similar p-type FET properties, strongly suggesting that GMGJs are responsible for the electrical characteristics in devices. More interestingly, because of the presence of photosensitive organic materials, reversible significant changes in current were observed when the devices were exposed to visible light. The responsivity we obtained in this work is as high as 8.3 A W$^{-1}$. At a rudimentary level, this study identifies that single-layer graphene sheets can serve as powerful electrodes, thus initiating worldwide research interest in making a wide variety of molecular

devices. Furthermore, because of their 2D compatibility with existing CMOS architectures, graphenes might be simply integrated into CMOS technology and find a broad application in developing integrated ultrasensitive devices at the nanometer scale.

## 4. Experimental

*Fabrication of Graphene-Based Transistors*: We obtained single-layer graphene sheets by a repeated peeling-off technique from natural kish graphites on a heavily doped silicon substrate with a 300 nm layer of thermally grown oxide. The identification of the single graphene sheets was performed by a combination of optical and atomic force microscopy. By using electron beam lithography, patterns with designed structures were formed on the top of graphenes. Metallic electrodes (3 nm of Cr followed by 40 nm of Au) were then deposited by thermal evaporator. The doped silicon wafer served as a global back-gate electrode for the devices.

*Formation of Cut Graphene Devices*: After the initial electric characterization of the devices, individual graphenes were then oxidatively cut by an ultrafine lithographic process and oxygen plasma etching that could produce the nanogaps between the graphene ends. In this study, we attempted to modify the fabrication procedure to control the gap size between the graphenes in the range of 100–150 nm. At first, a PMMA layer (950, A2) was spincast (4000 PRM, 45 s) on the surface and then baked at 170 °C for 2 min. Using electron beam lithography, we ran a DesignCAD file with around 100-nm-width line at the specific position to obtain the window precursor. Then a mixture of deionized (DI) water and isopropanol (1:3) was used for the liftoff at 5 °C for 1 min with the aid of sonication. After liftoff, the devices were washed by DI water and dried with a stream of $N_2$ gas. After the window was opened, the devices were put into a ME-3A RIE machine. The graphenes were then locally cut through the open window by oxygen plasma (50 W RF power, oxygen 300 mTorr, for 7 s). After cutting, the devices were soaked in acetone solution overnight, removed, washed by acetone, isopropanol, DI water, and dried with a stream of $N_2$ gas. Under these conditions, all the graphenes were completely cut with the gap size in the range of 100–150 nm. Parts of the devices were utilized further to fabricate the devices with graphene–metal junctions protected by PMMA using another electron beam lithographic process. It is in these small gaps that we deposited thin films of organic semiconductors.

*Formation and Characterization of Organic Nanotransistors*: Once cut graphene contacts were obtained, organic materials were deposited to form nanotransistors. P3HT thin-film devices [P3HT, poly(3-hexyl thiopene-2,5-diyl), Alfa Aesar] were achieved by immersing the open graphene circuits in its dilute chloroform solutions with different concentrations (0.50, 0.30, 0.28, and 0.25 mg $mL^{-1}$), and then removed from solution and dried under a stream of inert gas, while 40-nm pentacene thin-film transistors (Pentacene, Aldrich) were formed by standard thermal evaporation. The transistor characterization of these transistors was carried out at room temperature in the ambient atmosphere using an Agilent 4155C semiconductor characterization system and a Karl Suss (PM5) manual probe station. To initiate the photocurrent, we measured DC photoconductivity at room temperature in ambient atmosphere by illuminating the devices with visible light from a 150 W halogen lamp.

## Acknowledgements

We acknowledge primary financial support from FANEDD (no. 2007B21), MOST (2009CB623703), and NSFC (grant no. 50873004, 50821061, and 20833001). C. N. acknowledges financial support from the Nanoscale Science and Engineering Initiative of the National Science Foundation under NSF Award Number CHE-0641523 and by the New York State Office of Science, Technology, and Academic Research (NYSTAR). M. L. S. thanks the MRSEC Program of the National Science Foundation under Award Number DMR-0213574 for financial support. Supporting Information is available online from Wiley InterScience or from the author.

Received: March 10, 2009
Published online: June 22, 2009

[1] J. M. Tour, *Acc. Chem. Res.* **2000**, *33*, 791.
[2] A. K. Feldman, M. L. Steigerwald, X. Guo, C. Nuckolls, *Acc. Chem. Res.* **2008**, *41*, 1731.
[3] A. Nitzan, M. A. Ratner, *Science* **2003**, *300*, 138.
[4] A. H. Flood, J. F. Stoddart, D. W. Steuerman, J. R. Heath, *Science* **2004**, *306*, 2055.
[5] R. M. Metzger, *Ann. N. Y. Acad. Sci.* **2003**, *1006*, 252.
[6] N. J. Tao, *Nat. Nanotechnol.* **2006**, *1*, 173.
[7] Y. Selzer, D. L. Allara, *Ann. Rev. Phys. Chem.* **2006**, *57*, 593.
[8] Y. Zhang, J. R. Petta, S. Ambily, Y. Shen, D. C. Ralph, G. G. Malliaras, *Adv. Mater.* **2003**, *15*, 1632.
[9] J. Collet, O. Tharaud, A. Chapoton, D. Vuillaume, *Appl. Phys. Lett.* **2000**, *76*, 1941.
[10] J. B. Lee, P. C. Chang, J. A. Liddle, V. Subramanian, *IEEE Electron Device Lett.* **2005**, *52*, 1874.
[11] G. S. Tulevski, Q. Miao, M. Fukuto, R. Abram, B. Ocko, R. Pindak, M. L. Steigerwald, C. R. Kagan, C. Nuckolls, *J. Am. Chem. Soc.* **2004**, *126*, 15048.
[12] J. Robertson, *Mater. Today* **2007**, *10*, 36.
[13] S. E. Thompson, S. Parthasarathy, *Mater. Today* **2006**, *9*, 20.
[14] A. Lochtefeld, D. A. Antoniadis, *IEEE Electron Device Lett.* **2001**, *22*, 591.
[15] S. Iijima, *Nature* **1991**, *354*, 56.
[16] H. Dai, *Acc. Chem. Res.* **2002**, *35*, 1035.
[17] A. K. Geim, K. S. Novoselov, *Nat. Mater.* **2007**, *6*, 183.
[18] A. K. Geim, A. H. MacDonald, *Phys. Today* **2007**, *60*, 35.
[19] X. Guo, J. P. Small, J. E. Klare, Y. Wang, M. S. Purewal, I. W. Tam, B. H. Hong, R. Caldwell, L. Huang, S. O'Brien, J. Yan, R. Breslow, S. J. Wind, J. Hone, P. Kim, C. Nuckolls, *Science* **2006**, *311*, 356.
[20] A. C. Whalley, M. L. Steigerwald, X. Guo, C. Nuckolls, *J. Am. Chem. Soc.* **2007**, *129*, 12590.
[21] X. Guo, A. A. Gorodetsky, J. Hone, J. K. Barton, C. Nuckolls, *Nat. Nanotechnol.* **2008**, *3*, 163.
[22] P. Qi, A. Javey, M. Rolandi, Q. Wang, E. Yenilmez, H. Dai, *J. Am. Chem. Soc.* **2004**, *126*, 11774.
[23] K. Tsukagoshi, I. Yagi, Y. Aoyagi, *Appl. Phys. Lett.* **2004**, *85*, 1021.
[24] X. Guo, M. Myers, S. Xiao, M. Lefenfeld, R. Steiner, G. S. Tulevski, J. Tang, J. Baumert, F. Leibfarth, J. T. Yardley, M. L. Steigerwald, P. Kim, C. Nuckolls, *Proc. Natl. Acad. Sci. U. S. A.* **2006**, *103*, 11452.
[25] X. Guo, S. Xiao, M. Myers, Q. Miao, M. L. Steigerwald, C. Nuckolls, *Proc. Natl. Acad. Sci. U. S. A.* **2009**, *106*, 691.
[26] Y. Zhang, Y.-W. Tan, H. L. Stormer, P. Kim, *Nature* **2005**, *438*, 201.
[27] K. S. Novoselov, A. K. Geim, S. V. Morozov, D. Jiang, Y. Zhang, S. V. Dubonos, I. V. Grigorieva, A. A. Firsov, *Science* **2004**, *306*, 666.
[28] K. S. Novoselov, Z. Jiang, Y. Zhang, S. V. Morozov, H. L. Stormer, U. Zeitler, J. C. Maan, G. S. Boebinger, P. Kim, A. K. Geim, *Science* **2007**, *315*, 1379.
[29] F. Schedin, A. K. Geim, S. V. Morozov, E. W. Hill, P. Blake, M. I. Katsnelson, K. S. Novoselov, *Nat. Mater.* **2007**, *6*, 652.
[30] M. Y. Han, B. Oezyilmaz, Y. Zhang, P. Kim, *Phys. Rev. Lett.* **2007**, *98*, 206801.
[31] B. Ozyilmaz, P. Jarillo-Herrero, D. Efetov, D. A. Abanin, L. S. Levitov, P. Kim, *Phys. Rev. Lett.* **2007**, *99*, 166804.
[32] R. R. Nair, P. Blake, A. N. Grigorenko, K. S. Novoselov, T. J. Booth, T. Stauber, N. M. R. Peres, A. K. Geim, *Science* **2008**, *320*, 1308.
[33] L. A. Ponomarenko, F. Schedin, M. I. Katsnelson, R. Yang, E. W. Hill, K. S. Novoselov, A. K. Geim, *Science* **2008**, *320*, 356.
[34] N. Tombros, C. Jozsa, M. Popinciuc, H. T. Jonkman, B. J. van Wees, *Nature* **2007**, *448*, 571.
[35] D. A. Abanin, L. S. Levitov, *Science* **2007**, *317*, 641.
[36] R. Williams, L. DiCarlo, C. M. Marcus, *Science* **2007**, *317*, 638.
[37] X. Li, X. Wang, L. Zhang, S. Lee, H. Dai, *Science* **2008**, *319*, 1229.

[38] C. Lee, X. Wei, J. W. Kysar, J. Hone, *Science* **2008**, *321*, 385.
[39] B. Standley, W. Bao, H. Zhang, J. Bruck, C. N. Lau, M. Bockrath, *Nano Lett.* **2008**, *8*, 3345.
[40] K. I. Bolotin, K. J. Sikes, Z. Jiang, M. Klima, F. G. Udenberg, J. Hone, P. Kim, H. L. Stormer, *Solid State Commun.* **2008**, *146*, 351.
[41] S. V. Morozov, K. S. Novoselov, M. I. Katsnelson, F. Schedin, D. C. Elias, J. A. Jaszczak, A. K. Geim, *Phys. Rev. Lett.* **2008**, *100*, 016602.
[42] X. Du, I. Skachko, A. Barker, E. Y. Andrei, *Nat. Nanotechnol.* **2008**, *3*, 491.
[43] C. Di, D. Wei, G. Yu, Y. Liu, Y. Guo, D. Zhu, *Adv. Mater.* **2008**, *20*, 3289.
[44] N. Weste, K. Eshraghian, *Principles of CMOS VLSI Design: A Systems Perspective*, Addison Wesley Publishing Company, MA, USA **1985**.
[45] E. S. Yang, *Microelectronics Devices*, McGraw-Hill Inc., ON, USA **1988**.
[46] S. Gilje, S. Han, M. Wang, K. L. Wang, R. B. Kaner, *Nano Lett.* **2007**, *7*, 3394.
[47] S. Niyogi, E. Bekyarova, M. E. Itkis, J. L. McWilliams, M. A. Hamon, R. C. Haddon, *J. Am. Chem. Soc.* **2006**, *128*, 7720.
[48] C. D. Dimitrakopoulos, P. R. L. Malenfant, *Adv. Mater.* **2002**, *14*, 99.
[49] C. R. Kagan, P. Andry, *Thin-Film Transistors*, Dekker, New York **2003**.
[50] H. Ago, T. Kugler, F. Cacialli, W. R. Salaneck, M. S. P. Shaffer, A. H. Windle, R. H. Friend, *J. Phys. Chem. B* **1999**, *103*, 8116.
[51] W. M. H. Sachtler, G. J. H. Dorgelo, A. A. Holscher, *Surf. Sci.* **1966**, *5*, 221.
[52] H. E. Katz, Z. Bao, S. L. Gilat, *Acc. Chem. Res.* **2001**, *34*, 359.
[53] M. Raja, G. C. R. Lloyd, N. Sedghi, W. Eccleston, R. D. Lucrezia, S. J. Higgins, *J. Appl. Phys.* **2002**, *92*, 1441.
[54] H. Sakai, Y. Takahashi, H. *Appl. Phys. Lett.* **2007**, *91*, 113501.
[55] L. A. Majewski, M. Grell, *Synth. Met.* **2005**, *151*, 175.
[56] J. D. Meindl, *Proc. IEEE* **1995**, *83*, 619.
[57] K. S. Narayan, N. Kumar, *Appl. Phys. Lett.* **2001**, *79*, 1891.
[58] K. S. Narayan, S. Dutta, *Phys. Rev. B* **2003**, *68*, 125208.
[59] K. S. Narayan, S. Dutta, *Appl. Phys. Lett.* **2005**, *87*, 193505.
[60] M. C. Hamilton, S. Martin, J. Kanicki, *IEEE Trans. Electron Devices* **2004**, *51*, 877.